LLNL-JRNL-718467

A Comparison of Point Defects in Cd1-xZnxTe1-ySey Crystals Grown by Using Bridgman and Traveling Heater Methods

R. Gul, U. N. Roy, G. S. Camarda, A. Hossain, G. Yang, P. Vanier, J. Varley, V. Lordi, R. B. James

January 18, 2017

Journal of Applied Physics

Disclaimer

This document was prepared as an account of work sponsored by an agency of the United States government. Neither the United States government nor Lawrence Livermore National Security, LLC, nor any of their employees makes any warranty, expressed or implied, or assumes any legal liability or responsibility for the accuracy, completeness, or usefulness of any information, apparatus, product, or process disclosed, or represents that its use would not infringe privately owned rights. Reference herein to any specific commercial product, process, or service by trade name, trademark, manufacturer, or otherwise does not necessarily constitute or imply its endorsement, recommendation, or favoring by the United States government or Lawrence Livermore National Security, LLC. The views and opinions of authors expressed herein do not necessarily state or reflect those of the United States government or Lawrence Livermore National Security, LLC, and shall not be used for advertising or product endorsement purposes.

LLNL-JRNL-718467

A Comparison of Point Defects in $Cd_{1-x}Zn_xTe_{1-y}Se_y$ Crystals Grown by Bridgman and Traveling Heater Methods

R. Gul[a,b], U. N. Roy[a], G. S. Camarda[a], A. Hossain[a], G. Yang[a], P. Vanier[a] V. Lordi[c], J. Varley[c] and R. B. James[a,d]

[a]Brookhaven National Laboratory, Upton, NY, USA

[b]Alabama A&M University, Normal, AL, USA

[c] Lawrence Livermore National Laboratory, Livermore, CA 94550, USA

[d]Savannah River National Laboratory, Aiken, SC 29808, USA

Keywords: CdZnTeSe, point defects, carrier trapping, iDLTS, deep levels, radiation detectors

ABSTRACT

In this paper, the properties of point defects in $Cd_{1-x}Zn_xTe_{1-y}Se_y$ (CZTS) radiation detectors are characterized using deep-level transient spectroscopy and compared between material grown using two different methods, the Bridgman Method and Traveling Heater Method. The nature of the traps was analyzed in terms of their capture cross-sections and trap concentrations, as well as their effects on the measured charge-carrier trapping and de-trapping times, and then compared for the two growth techniques. The results revealed that the Se addition to CdZnTe can reduce the V_{Cd}^{--} concentration. In THM and BM grown CZTS detectors,

besides a few similarities in the shallow and medium energy traps, there were major differences in the deep traps. It was observed that the excess-Te and lower growth-temperature conditions in THM-grown CZTS led to a complete compensation of V_{Cd}^{--} and two additional traps (attributed to Te_i^{-} and Te_{Cd}^{++} appearing at around $E_v + 0.26$ eV and $E_c - 0.78$ eV, respectively). The 1.1-eV deep trap related to large Te secondary phases was a dominant trap in the BM-grown CZTS crystals. In addition to i-DLTS data, the effects of point defects induced due to different processing techniques on the detector's resistivity, spectral response to gammas, and $\mu\tau$ product were determined.

I. INTRODUCTION

For decades, researchers have investigated means to improve the crystal quality of CdTe and its alloys for use in room-temperature radiation detectors for applications in nonproliferation, national security, medical imaging, and space imaging, in addition to interest in semiconductor and optoelectronic technologies[1,2,3]. CdTe and its alloys with Zn (CdZnTe or CZT) have been effectively used for detectors, sensors, and substrates for infrared imaging applications, but there are still some drawbacks of the material that have been difficult to fully overcome[4]. Most of the issues arise from the melt-growth techniques used for synthesis of large, nearly single crystals. For CdTe-based alloys incorporating Zn, which are advantageous for increasing the band-gap of room-temperature detectors, obtaining desirable crystal uniformity is complicated by a significant variation in the Zn concentration along the ingot growth direction due to the segregation coefficient of Zn in the CdTe matrix being greater than 1. In addition, CZT growth by melt solidification causes various types of extended defects to form, such as stacking faults, twins, dislocations, and sub-grain boundaries and their networks[5]. To achieve the required high resistivity for room-temperature detector applications, crystals are grown under a Te-rich

atmosphere, which can cause the generation of Te-rich secondary phases (Te_{SP}), especially Te inclusions, during the crystal growth. These secondary phases affect the quality, uniformity and performance of the detectors to various degrees, depending on their concentration and size[6]. Furthermore, point defects at the microscopic level control the resistivity of the material and performance of the detectors by inducing deep traps, which play an important role as trapping and recombination centers for the charge carriers[7].

To obtain a high yield of high-quality material, the control of defects in CdTe and its alloys must be addressed. One common approach is to employ new or modified crystal-growth and purification techniques. Another option is to modify the chemical composition of CdTe and its alloys, particularly by adding new dopants and/or additional alloy constituents. Due to widespread drive for detector improvements, crystal growers, researchers and vendors have searched for alternative materials having fewer microscopic and macroscopic defects compared to CZT, in addition to taking steps to improve the processes used to grow and purify CZT. Several related alternative materials have been investigated, including CdMnTe[8], CdTeSe[9,10], and CdMgTe[11]. Recently, Se was added to CZT to achieve improved crystallinity of CdZnTeSe crystals and comparable electron lifetimes compared to CZT. In this research, the focus is on the point defects induced in CdZnTeSe crystalline material grown by two different techniques, Bridgman Method (BM) and Travelling Heater Method (THM).

II. EXPERIMENTAL DETAILS

In this research, we investigated two sets of detectors: In-doped high resistivity CZTS grown by BM and by THM. The BM-grown detector (CZTS:BM) contains 2% Se with a composition of $Cd_{0.9}Zn_{0.1}Te_{0.98}Se_{0.02}$, while the THM-grown sample (CZTS:THM) contains 7%

Se with a composition of $Cd_{0.9}Zn_{0.1}Te_{0.93}Se_{0.07}$. The growth temperature for the THM method was about 850 ^{0}C, while, for BM growth, the temperature was raised about 20 ^{0}C above the melting point of CZT (~1120 ^{0}C) and then the ampoule was lowered for solidification. One of the main differences in the growth of these two types of crystals was the additional Te-rich conditions and lower growth temperature in the case of CZTS:THM. The CZTS crystals used for this research were grown at Brookhaven National Laboratory. The crystallinity of the CZTS was better than CZT crystals, and there were less detrimental defects due to a reduction of sub-grain boundaries and their networks and a reduced concentration of Te-rich secondary phases. In addition the compositional homogeneity of Zn was better than for CZT, and the Se composition of the CZTS was highly uniform. Details of the crystal growth process will be published later.

Planar detectors were made by fabricating Au contacts on two opposing planar sides using an electroless technique. The dimensions of the detectors are reported in Table I. The resistivity of the detectors was determined from I-V measurements, which helped to define the electrical parameters and temperature range for the photo-induced current deep-level transient spectroscopy (iDLTS) experiments used to characterize the point defects. The spectral response was tested using an ^{241}Am standard source. The mobility-lifetime ($\mu\tau$) products were measured from the charge-collection data at different applied biases for the two detectors followed by fitting to the Hecht equation.

Details of the iDLTS system and the experimental and analytical procedures are described elsewhere by Gul et al.[12] An improved illumination set-up using an 850-nm diode laser with optimized power and better alignment with a laser spot of about 1 mm was used for the filling of traps. The laser pulse parameters were 2-mm width and 1-s period with a 10-ns pulse

rise time. The use of a 1-s period is beneficial to collect more of the long tail of the transient current due to slow de-trapping from some of the deep traps.

To obtain good statistical data, iDLTS experiments were run four times for each sample, including a first run from 10 to 300 K (RT-run), and then three runs from 10 to 400 K (above RT-run). The first two runs helped in evaluating the changes due to the above-RT heating (up to 400 K) on the shallow traps (< 100 K). The values for energy levels and capture cross-sections for the traps were calculated based on averaged values obtained from all four runs.

This research focus on the differences and similarities in the nature of the traps induced in CZTS crystals due to the two different growth techniques and the corresponding concentrations of these traps. Point defects and their effects on the charge carrier lifetimes were evaluated by measuring the trapping and de-trapping times. In addition, the effects of point defects induced by the two growth techniques on the resistivity, spectral response to gammas, and $\mu\tau$ product were investigated.

In addition to CZTS detectors two In-doped CZT BM and THM detectors were characterized for point defects. The additional data helped to understand growth-related point defects for the two methods and the effects associated with the addition of Se in BM- and THM-grown CZT detectors.

III. RESULTS and DISCUSSION

1. Properties and Detector Response

The data for resistivity, spectral response to incident ^{241}Am gamma-rays, and the $\mu\tau$ product for two detectors are listed in Table I. The CZTS:BM detector shows one order of magnitude higher resistivity (1×10^{10} Ω-cm) than the CZTS:THM ($\sim2\times10^{9}$ Ω-cm) detector, but

despite the higher resistivity, the CZTS:BM detector showed no photocurrent response to white light or to gammas. On the other hand, the CZTS:THM detectors, even with their lower resistivity, showed a gamma response from which it was possible to extract a μτ-product value of ~1-2x10^{-3} cm^2/V-s. Infrared microscopy was used to examine the Te secondary phases in the two detectors. The concentration of big Te secondary-phase particles (diameters between 10 and 25 μm) in CZTS:THM were between 10^2-10^3 cm^{-3}, while in CZTS:BM, it was an order of magnitude larger (i.e., 10^3-10^4 cm^{-3}). The density of Te secondary phase particles sized below 10 μm in CZTS:THM detectors (~10^5 cm^{-3}) was ~1 order of magnitude higher than in the CZTS:BM. The comparison of structural, defects, and electrical transport properties shown in Table I suggests that the electron μτ product and lifetime are mainly correlated with the larger Te secondary-phase particles with size > 10 μm.

2. Point Defects in Detectors

iDLTS data for the two CZTS detectors are plotted in Figures 1-5. There were a few similarities as well as some differences in the type and nature of the point defects. The identified traps in the two detectors are listed in Table II. The details of the defects levels (E_t, shown in Fig. 1,2), their densities (N_t, shown in Fig. 3), and their capture cross-sections (σ, shown in Fig. 4), in the two differently-grown CZTS detectors are described in the following sections:

(a). CZTS:BM. The iDLTS plots for CZTS:BM detectors are shown in Fig. 1a, where the inset shows the Arrhenius plot for 1000/KT vs. log(T^2t_1); herein, t_1 is the starting time for the time-current window for the transient collected at temperature T. The first four traps, as shown in Figs. 1a and 1b, are identified as the same traps in both THM- and BM-grown CZTS detectors.

The difference can be seen only in the amplitudes of the signals, which is one of the key parameters affecting the densities of traps (Fig. 3).

Two shallow traps in the temperature scan below 100 K were identified at 23 and 57 meV with an occupational density of 6 $x10^{11}$ and $5x10^{11}$ cm^{-3}, respectively. The value for the capture cross section σ shown in Fig. 4 for the first shallow trap is very small (i.e., less than 10^{-19} cm^2). The second shallow trap at 57 meV has a considerably higher σ of ~10^{-17} cm^2. This trap is found in both CZTS detectors, but was not identified in CZT detectors in our previous reported research[13,14]. Thus, there is a high probability that the 57-meV trap is related in some manner to a shallow donor induced by the addition of Se into CZT. In the temperature range 100-300 K, two medium level traps with energies at 0.18 eV (A-center) and 0.26 eV (most probably related to Te interstitials (Te_i^-)) are observed. It was observed that the shallow traps in BM-grown CZTS detectors were present with slightly lower densities compared to THM-grown detectors. The densities of A-centers (0.18 eV) for both growth methods were very similar ~$1x10^{11}$ cm^{-3}, while Cd vacancies (V_{Cd}^{--}) for BM-grown CZTS were present with lower density (~ $4x10^{10}$ cm^{-3}) than for THM-grown material. For the deep traps, in BM-grown CZTS the 1.1-eV trap (labeled as Te_{SP}) was present with higher density (~$4x10^{11}$ cm^{-3}) for large-size (~30 μm) secondary phases, but the method was observed to correlate with much lower densities of Te_i ($2x10^{10}$ cm^{-3}) and Te_{Cd}^{++} (below detection). These observations suggest a connection between large (20-30 μm diameter) Te-rich phases and the 1.1-eV trap. The inability to quantify the electron charge collection prevented a measurement of the electron μτ product from that sample. These results indicate that an excess of the Te_{SP} deep trap (and hence large Te-rich phases of ~30-μm size) generates more detrimental electron trapping centers in the BM-grown as compared to the THM-grown CZTS crystal. Such explanation does not hold for CZT. Additional growth runs and

further studies are being carried out to improve the CZTS quality and provide additional data to strengthen the analysis of our observations.

(b) CZTS:THM. Point defects in these detectors are shown in Fig. 1b. Arrhenius plots are shown in the inset. Five different traps were identified, although some data above 350 K was probably masked due to the higher leakage current. This higher noise level makes it hard to distinguish the Te_{SP} trap (expected in the 350-400 K temperature range where the dark current begins to increase rapidly with temperature), particularly when it has a relatively low density.

Regarding shallow traps, two were clearly identified around 23 and 57 meV with density of $3x10^{11}$ and $4\ x10^{11}\ cm^{-3}$, respectively, as shown in Fig. 3b. The four traps identified below 300 K were similar to the traps identified in CZTS:BM, but with different occupied densities. For the levels below 300 K in CZTS:THM, the concentrations were about an order of magnitude higher density ($\sim10^{11}\ cm^{-3}$) compared to CZTS:BM ($\sim10^{10}\ cm^{-3}$), except for the A-center. Above room temperature, one deep trap at ~0.78 eV was identified, which is due to the occupancy of Te on a Cd lattice point, which causes the Te_{Cd}^{++} energy trap. The density for Te_{Cd}^{++} in THM-grown CZTS was almost the same as V_{Cd}^{--} in BM-grown CZTS. This indicates that nearly all V_{Cd}^{--} in THM-grown CZTS were replaced by Te, forming a Te anti-site (Te_{Cd}^{++}). In addition, the density of the Te_i-related trap at around 0.26 eV increased by a factor of ten in CZTS:THM.

Beside the similarities in energy traps identified below RT, there are a few major differences between BM- and THM-grown CZTS, especially in the high-temperature region. In BM-grown crystals, there was no measurable Te_{Cd}^{++} (0.73 eV), and instead there were two additional traps: one labeled as V_{Cd}^{--} at around 0.37 eV and another the well-known 1.1-eV Te secondary-phase related trap found in most of the CdTe-based alloyed detectors. The capture

cross-section σ as shown in Fig. 4 for the traps at 0.37 eV and 1.1 eV has the value of about 10^{-15} and 10^{-10} cm^2, respectively. The 1.1-eV trap is the dominant trap at room temperature amongst all traps identified in BM-grown CZTS detectors.

After making the analysis of the traps and comparing their corresponding occupational densities, as well as the expected origins of traps, it appears that V_{Cd}^{--} and Te_{SP} play important roles in generating interstitials or complexes with V_{Cd}^{--}. Their conversion and relative variation in densities with the growth process establish a dynamics between the traps, possibly driven more completely during the higher-temperature growth used for BM-grown CZTS. A simple sketch of the trap conversion dynamics is illustrated in Fig. 5, indicating the role of V_{Cd}^{--} in complexing with the interstitials/dopants/impurities and combining with the Te secondary phases, causing the relative concentrations of the deep-level point defects to differ substantially for the two growth methods.

The data and description given above indicate that the excess Te in THM-grown CZTS occupies two different levels: Te_i^- and Te_{Cd}^{++}. This might be one of the reasons for little or no V_{Cd}^{--} (fully compensated) and a negligibly low density of Te_{SP}, although the lower growth temperature for THM may also be important. In addition, the lower resistivity and negligible concentration of the 1.1-eV trap appear to be correlated. These data provide additional evidence that the 1.1-eV trap is connected to big size (≥ 25 μm in diameter) Te-rich secondary phases. Based on the iDLTS point defect data evaluated for the two growth methods, a proposed energy band diagram showing the traps within the band-gap in CZTS crystals is shown in Fig. 6.

3. Comparison of Traps between CZTS and CZT Detectors

To show the effects of Se addition on point defects in CZT, we include the iDLTS plots for In-doped CZT detectors grown by the BM- and THM- technique, as shown in Fig. 2. To make the comparisons more clear, the results are also presented in Table 2. There are similarities and differences in the traps identified by iDLTS in In-doped CZTS and CZT detectors. The shallow traps in CZT and CZTS are almost the same and may be an indication of the presence of In dopants present in both materials. The second shallow level is the A-center, which was identified in all three detectors, except for CZT:BM, which might be due to CZT:BM growth conditions favoring the generation of Cd vacancies (V_{Cd}^{--}) instead of their complex with an In dopant to form an A-center (V_{Cd}^{--} - In_{Cd}). A major difference in traps was observed in the medium energy traps, see Figs. 1 and 2. The Se addition causes the generation of a new trap at around 0.26 eV in both CZTS BM- and THM-grown detectors. In addition V_{Cd}^{--}, which has a trap level at ~ 0.37 eV, is completely compensated in CZTS. The deep trap at ~ 1.1 eV was identified in all three detectors except for CZTS:THM. It seems that THM growth and the addition of Se (i.e., CZTS crystals) was successful to eliminate the 1.1-eV deep trap. The presence of the 1.1-eV trap helped to achieve high resistivity in CZTS:BM, CZT:BM, and CZT:THM. The good gamma response for CZTS:THM, even with comparably lower resistivity, indicates that Se addition and use of the THM growth method is more effective for room-temperature radiation detectors applications. There is still need to improve the quality of crystals by increasing the electrical resistivity and the response towards gamma radiation.

4. Charge Trapping in Defects

We calculated the times for trapping (t_t) and de-trapping (t_{dt}) of charge carriers for each trap from the iDLTS data. The values for t_t are calculated by were calculated using the modified Shockley-Read-Hall model, for CdTe-based alloys:[15]

$$t_t \sim [N_t V_{th} \sigma]^{-1}.\{1+10^{-5}\cosh\{(E_t-E_i)/k_B T\} \qquad (1)$$

Here, E_t is the energy of the point-defect level of the trap, E_i is the intrinsic Fermi level, k_B is the Boltzmann constant, T is the temperature (room temperature (RT) used to correspond to detector operation), and V_{th} is the thermal velocity of the carriers at RT. As the resistivity of the CZTS detectors investigated in this research was between 10^9 – 10^{10} Ω-cm, the free charge carrier density was estimated at 10^5 carriers per cm^3 in equation 1, instead of 10^6 carriers per cm^3. The values for t_{dt} are determined from the emission rate (e_n) of the charge carriers from the laser-filled traps.

The data showing the variation of t_t and t_{dt} with the corresponding energies for the different traps are plotted in Fig. 7. The values for t_t decrease monotonically with increasing activation energies of the traps, as illustrated by the plots. It can be observed that the deep traps are faster in trapping the charge carriers than the shallow traps. The two regions shown in Fig. 7 can be described as below:

RI: The t_t and t_{dt} are almost same at an energy level of ~ 0.45 eV. In the region of shallow and medium energy traps having $E_t \leq 0.45$ eV, the t_t are longer than the t_{dt} ($t_t > t_{dt}$). It means in this region there will be little or no effect on the charge collection (except for E_t greater than about 0.40 eV), and hence negligible effect on the carrier lifetime or μτ-product.

RII: For deep-level traps having $E_t > 0.45$ eV, t_t is shorter than the t_{dt} ($t_t < t_{dt}$), hence trapping is faster, while the emission rates from these deep traps are slow and often delayed well beyond the data acquisition time. For most of these deep levels, the difference reaches to minutes, and the charge carriers are completely lost before the signal can be counted. In this

case, the deep traps have a major contribution to charge loss and have a remarkable effect on the carrier lifetimes; hence, they have a major contribution in lowering the μτ-product.

Summarizing the trapping and de-trapping dynamics of the different defects in each detector, the Te_i^- trap in CZTS:THM has a value for t_t more than four orders of magnitude higher than t_{dt} (clearly RI, which indicates a negligible role as a trapping center for detectors operating at room temperature), while for CZTS:BM, the trapping and de-trapping times are closer (about 1-2 orders of magnitude different). In CZTS:THM, Te_{Cd}^{++} plays a dominate role in killing charge carriers and ultimately the μτ, since the values of t_t and t_{dt} are, respectively, less than 0.1 μs and more than 10 ms, respectively; this defect does not appear in CZTS:BM in an appreciable concentration. Instead, in CZTS:BM, Te_{SP} has t_t in ns and very high t_{dt} (in minutes), possible dominating the electron charge loss as the major trapping center and killing the detector response. Also, in CZTS:BM, the V_{Cd}^{--} has a value of t_t < ms, and t_{dt} is 2 orders shorter, thus having no significant contribution to μτ.

CONCLUSIONS

In this work, we characterized two types of In-doped CZTS detectors (i.e., crystals grown by the Bridgman growth method and by the Traveling Heater Method). Distinct shallow, medium and deep energy traps were identified for each growth method. CZTS crystals, as compared to CZT, have a relatively low concentration of V_{Cd}^{--}. It indicates that the Se addition to CZT can be used for effective compensation of V_{Cd}^{--}. Traps with energy levels > 0.5 eV are mainly limiting the lifetime of charge carriers. A deep trap at 1.1 eV due to Te_{SP} (>10-μm diameter in size) helps to achieve high resistivity in CZTS crystals, but at the same time the high density of this deep level generates more trapping/recombination centers that kill the μτ product

and cause a degradation of the detector response. For example, the CZTS:BM detector showed a high density of the 1.1-eV trap and a high resistivity of 2×10^{10} Ω-cm, but the short trapping time kills the carrier lifetime, and the detector showed no response to gamma rays. The case is opposite for the CZTS:THM detector, where we found no 1.1-eV trap, and the detector showed good response towards gammas. The data on point defects, high electrical resistivity, and high $\mu\tau$ values for electrons in CZTS suggest that it is a promising potential alternative material to CZT for high-performing room-temperature radiation detectors.

ACKNOWLEDGMENTS

This work was supported by the U.S. Department of Energy, Office of Defense Nuclear Nonproliferation Research and Development, DNN R&D. The manuscript was authored by Brookhaven Science Associates, LLC under Contract No. DE-AC02-98CH10886 with the U.S. Department of Energy. Part of this work was performed under the auspices of the U.S. Department of Energy by Lawrence Livermore National Laboratory under Contract DE-AC52-07NA27344.

REFERENCES

1. T. E. Schlesinger, J. E. Toney, H. Yoon, et al., *Materials Science and Engineering R* **32**, 103 (2001); http://dx.doi.org/10.1016/S0927-796X(01)00027-4.
2. C. Szeles, "CdZnTe and CdTe materials for X-ray and gamma ray radiation detector applications," *Phys. Stat. Sol. (b)* **241**, no. 3, 783 (2004); DOI: 10.1002/pssb.200304296.
3. H. Chen, S. A. Awadalla, K. Iniewski, et al., *J. Appl. Phys.* **103**, 014903 (2008); http://dx.doi.org/10.1063/1.2828170.
4. P. Rudolph, *Cryst. Res. Technol.* **38**, no. 7–8, 542 (2003); DOI: 10.1002/crat.200310069.

5. A. E. Bolotnikov, S. Babalola, G. S. Camarda, et al., *IEEE Trans. on Nucl. Science* **58**, No. 4, 1972 (2011); DOI: 10.1109/TNS.2011.2160283.
6. A. E. Bolotnikov, S. Babalola, G. S. Camarda, et al., *IEEE Trans. on Nucl. Science* **57**, Issue 2, 910 (2010); DOI: 10.1109/TNS.2010.2042617.
7. R. Gul, U. N. Roy, S. U. Egarievwe, et al., *J. Appl. Phys.* 119, 025702 (2016); DOI: 10.1063/1.4939647.
8. U. N. Roy, G. S. Camarda, Y. Cui, et al., *J. Crystal Growth* **437**, 53 (2016); http://dx.doi.org/10.1016/j.jcrysgro.2015.12.017.
9. U. N. Roy, A. E. Bolotnikov, G. S. Camarda, et al., *APL Mater.* **3**, 026102 (2015); doi: 10.1063/1.4907250.
10. R. Gul, U. N. Roy, A. E. Bolotnikov, et al., *APL Mater.* **3**, 040702 (2015); doi:10.1063/1.4917270.
11. Sudhir B. Trivedi et al., "Next Generation Semiconductor-Based Radiation Detectors Using Cadmium Magnesium Telluride", Report for DOE, November 17, 2014.
12. R. Gul, A. E. Bolotnikov, K. H. Kim, et al., *J. Electron. Mater.* **40**, 274 (2011); DOI: 10.1007/s11664-010-1504-x.
13. R. Gul, U. N. Roy and R. B. James, "Point defects in Bridgman Grown In-, Al-, Ni-, and Sn-doped CdZnTe detector, and their effects on resistivity and trapping times", *J. Appl. Phys.* **121**, 11 (2017).
14. R. Gul, K. Keeter, R. Rodriguez , et al., "Point Defects in Pb-, Bi- and In-doped CdZnTe Detectors: Deep Level Transient Spectroscopy (DLTS) Measurements", *J. Electron. Mater.* **41**, No. 3, 488 (2012); doi:10.1007/s11664-011-1802-y

15. G. Tepper, R. Kessick and C. Szeles, *Proc*. *SPIE*, **4507**, in Hard X-Ray and Gamma-Ray Detector Physics III, 79 (SPIE, Bellingham, WA, 2001); DOI:10.1117/12.450744.

TABLE I. Detector specifications, structural and electrical-transport properties

Detector	Dimensions l x w x t (mm^3)	Average Concentration of Te_{SP} (cm^{-3})	Size of Dominant Te_{SP} (μm)	Resistivity (Ω-cm)	γ-ray Response	$\mu\tau_e$ cm^2/V-s
$Cd_{0.9}Zn_{0.1}Te_{0.98}Se_{0.02}$ (BM)	5.5x5.1x3.7	$8x10^4$	0-30	$1x10^{10}$	No	--
$Cd_{0.9}Zn_{0.1}Te_{0.93}Se_{0.07}$ (THM)	5.0x4.2x2.3	$3x10^5$	0-10	$2x10^9$	Yes	$1-2x10^{-3}$
$Cd_{0.9}Zn_{0.1}Te$ (BM)	3.6x3.3x1.1	--	--	$9x10^9$	Yes	$0.4x10^{-3}$
$Cd_{0.9}Zn_{0.1}Te$ (THM)	9.5x9.6x1.8	--	--	$1x10^{10}$	Yes	$1x10^{-3}$

TABLE II. Traps identified in CZTS, and CZT detectors, their expected origins and capture cross-sections (σ).

E_t	**Expected Origin of the Trap**	**σ (cm^2)**	**Detectors**			
			CZTS (BM)	**CZTS (THM)**	**CZT (BM)**	**CZT (THM)**
Ec-22 meV	Donor impurities	9×10^{-21}	√	√	x	20 meV
Ec-58 meV	Se-related donor	5×10^{-17}	√	√	50 meV	45 meV
Ev+0.18 eV	A-center	1×10^{-16}	√	√	x	√
Ev+0.26 eV	Te_i^-	1×10^{-14}	√	√	x	x
Ev+0.37 eV	V_{Cd}^{--}	1×10^{-15}	√	x	√	√
Ec-0.78 eV	Te_{Cd}^{++}	5×10^{-11}	x	√	√	x
Ev+1.1 eV	Te_{SP}	1×10^{-10}	√	x	√	√

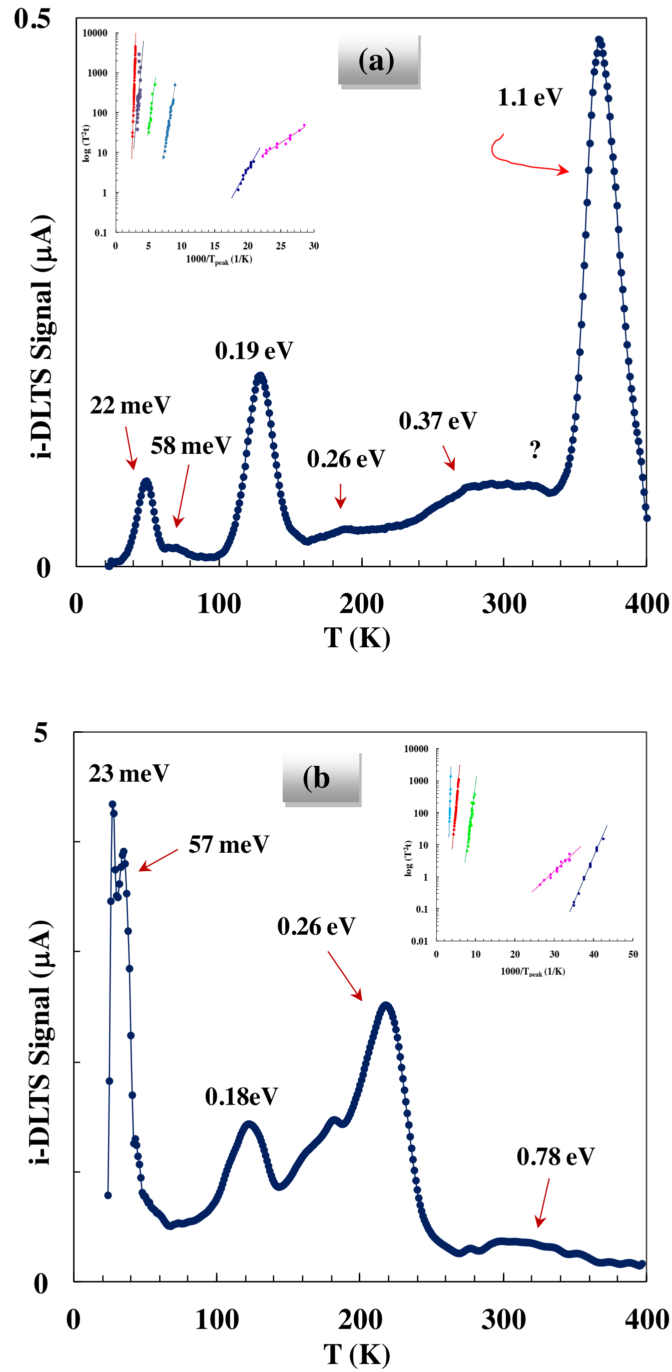

FIG. 1. iDLTS plots showing point defects for two different time windows with a 2-ms pulse width at 1-V applied bias for: (a) CZTS:BM and (b) CZTS:THM. Arrhenius plots are shown in the insets.

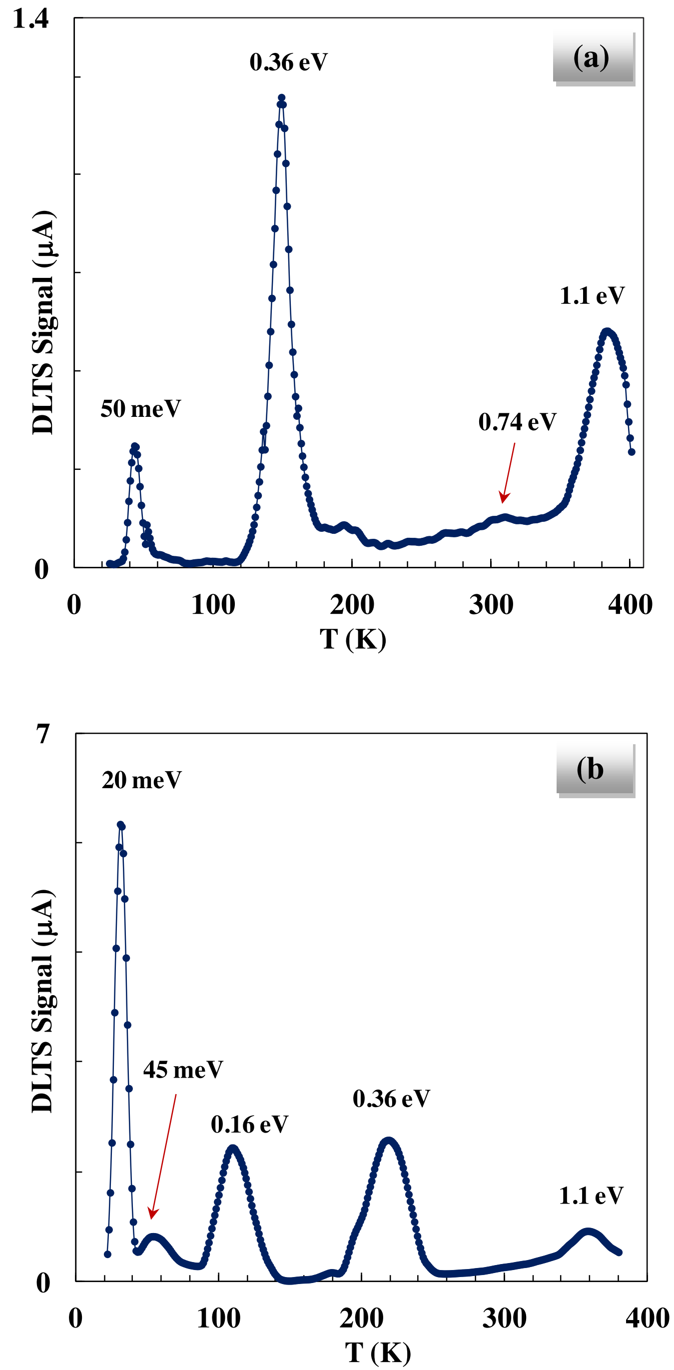

FIG. 2. iDLTS plots showing point defects for two different time windows with a 2-ms pulse width at 1-V applied bias for: (a) CZT:BM and (b) CZT:THM.

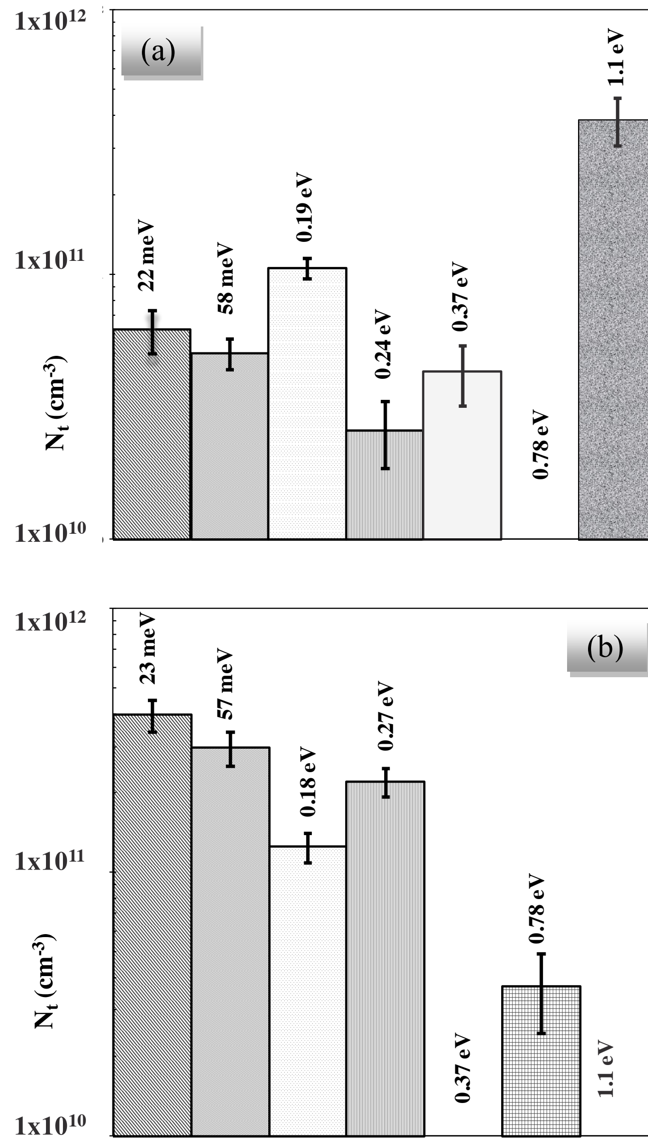

FIG. 3. Comparison of the densities of point defects in: (a) CZTS:BM and (b) CZTS:THM.

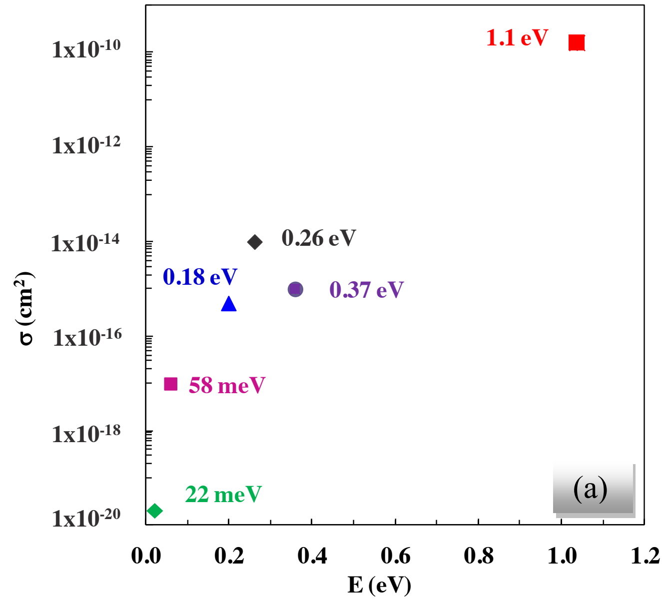

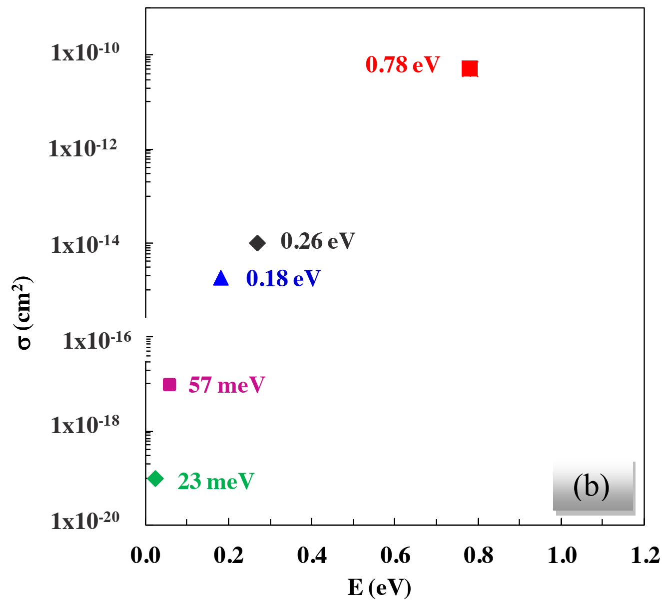

FIG. 4. Capture cross-sections for the charge carriers for traps identified in: (a) CZTS:BM and (b) CZTS:THM.

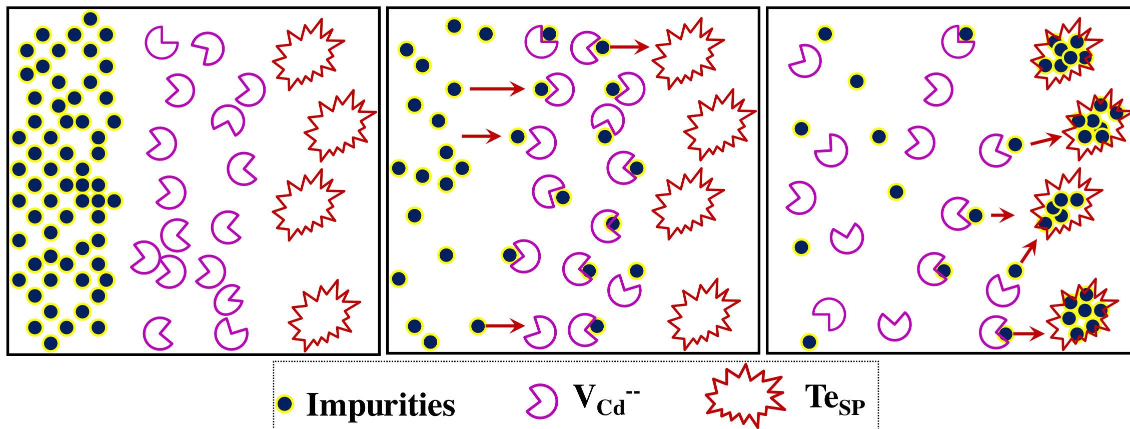

FIG. 5. Proposed model for the role of Te secondary phase (gettering centers), Cd vacancies, interstitial Te and impurities in the point-defect formation in CZTS.

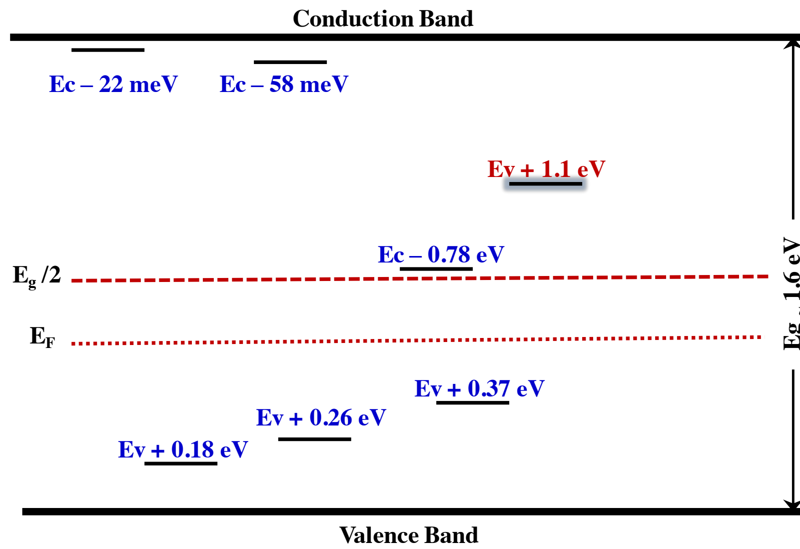

FIG. 6. Proposed band diagram for CZTS crystals based on the energy levels identified by iDLTS.

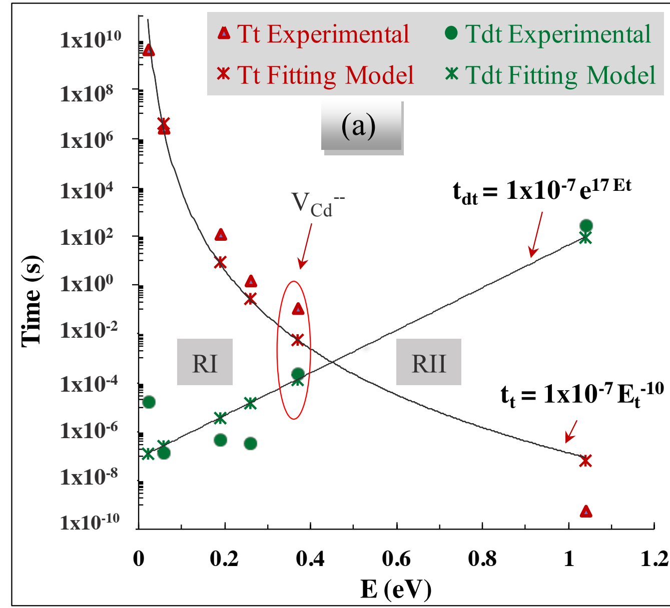

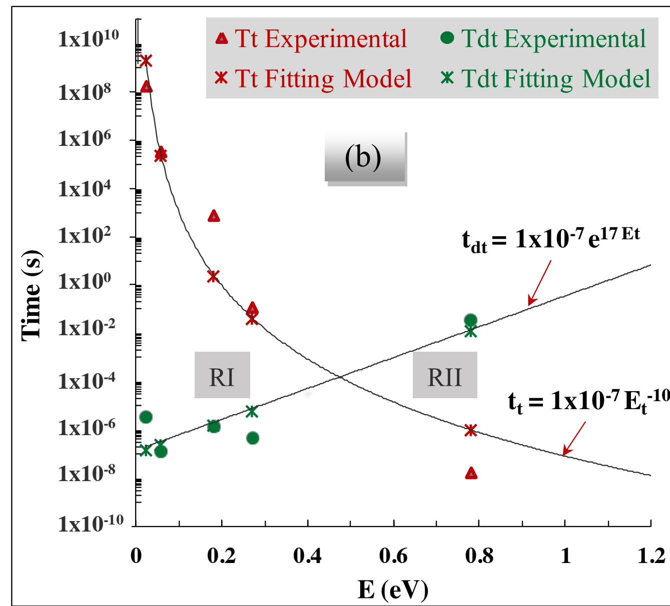

FIG. 7. Trapping and de-trapping times of point defects for the charge carriers in (a) CZTS:BM, and (b) CZTS:THM detectors.